Heterogeneous Catalysis

International Edition: DOI: 10.1002/anie.201410093
German Edition: DOI: 10.1002/ange.201410093

Active Sites and Mechanisms for Direct Oxidation of Benzene to Phenol over Carbon Catalysts**

*Guodong Wen, Shuchang Wu, Bo Li, Chunli Dai, and Dang Sheng Su**

Abstract: *The direct oxidation of benzene to phenol with H_2O_2 as the oxidizer, which is regarded as an environmentally friendly process, can be efficiently catalyzed by carbon catalysts. However, the detailed roles of carbon catalysts, especially what is the active site, are still a topic of debate controversy. Herein, we present a fundamental consideration of possible mechanisms for this oxidation reaction by using small molecular model catalysts, Raman spectra, static secondary ion mass spectroscopy (SIMS), DFT calculations, quasi in situ ATR-IR and UV spectra. Our study indicates that the defects, being favorable for the formation of active oxygen species, are the active sites for this oxidation reaction. Furthermore, one type of active defect, namely the armchair configuration defect was successfully identified.*

Carbon is emerging as an important non-metal catalyst for many heterogeneous catalysis, including thermocatalysis (e.g., dehydrogenation of ethylbenzene and alkanes,[1] oxidation of ethylbenzene and cyclohexane,[2] oxidation of alcohol,[3] and hydrogenation of olefin[4]), photocatalysis[5] and electrocatalysis.[6] Although a great number of carbon catalysts have been developed in the recent years, the understanding of reaction mechanism of carbon catalysts, and especially the identification of the active sites, has been restricted owing to the complex surface structure (e.g., defect, amorphous carbon and graphitized carbon), co-existence of various functional groups, and the presence of metal impurities.[7] We have made great efforts to show that the carbonyl group is the active site in the oxidative dehydrogenation of hydrocarbons (e.g., ethylbenzene and light alkanes) and reduction of nitrobenzene.[1a,b,7b,8]

Transformation of arenes into value-added oxygen-containing compounds under mild conditions, such as by the oxidation of benzene to phenol, is one of the most active topics in applied and fundamental catalytic research.[9] Considering that benzene is very difficult to activate, the phenol yield is relatively low in most of the reported cases, therefore the conversion of benzene into phenol is a challenge. The direct oxidation of benzene to phenol with H_2O_2 as the oxidizer is an alternative process to the commercial cumene route.[10] Although carbon catalysts are reported as promising catalysts in this process, the active sites and mechanisms are still a topic of controversy. Whether the activity is attributed to oxygenated groups, curved sp^2-hybridized carbon surface, defects, or graphene layers has been a topic of intense debate.[11] Herein, the catalytic process was studied by using small organic molecular model catalysts, Raman spectra, SIMS, DFT calculations, quasi in situ ATR-IR and UV spectra. The results demonstrated that the defects, which were favorable for the formation of active oxygen species, were the active sites. We also identified that the armchair configuration defect was one type of active defect.

Firstly, the catalytic performance of various kinds of carbon materials was studied (Table 1), including carbon nanotube (CNT7000), activated carbon, flake graphite (FG7-10), nanodiamond, and acetylene black. Carbon nanotube (CNT) gave a significantly higher phenol yield than other carbon catalysts. Although the carbon nanotube had been pretreated in concentrated HCl for 20 h to reduce metal residues, the metal impurities could not be completely removed, thus the catalytic role of metal residues could not be simply excluded. However, the phenol yield did not decrease when the carbon nanotube was washed with HCl again for a longer time, indicating that the activity mainly originated from the carbon itself. Flake graphite is a natural carbon materials with negligible metal impurities,[3b] and we still got 1.4% phenol yield over this catalyst. This is in good agreement with the conclusion of Yang and co-workers who reported that the activity for the benzene oxidation was not ascribed to the metal residues but the carbon itself.[11a]

Table 1: Direct oxidation of benzene over different carbon catalysts.[a]

Catalysts	Phenol yield [%]	Phenol selectivity [%]
CNT7000	5.8	91.5
Activated carbon	1.7	90.9
FG7-10	1.4	89.1
Nanodiamond	0.4	72.4
Acetylene black	0.1	100.0
Blank[b]	-	-

[a] Reaction conditions: 60 °C, 6 h, 50 mg catalyst, 0.5 mL benzene, 10 mL acetonitrile, H_2O_2/benzene molar ratio is 2. [b] Conducted in the absence of catalyst: no phenol was detected.

Then we studied the mechanism especially what was the active sites of carbon catalysts. The catalytic performance of

[*] Dr. G. D. Wen, Dr. S. C. Wu, Dr. B. Li, Dr. C. L. Dai, Prof. Dr. D. S. Su
Shenyang National Laboratory for Materials Science, Institute of Metal Research, Chinese Academy of Sciences
72 Wenhua Road, Shenyang 110016 (China)
E-mail: dssu@imr.ac.cn

[**] This work is financially supported by Doctoral Starting up Foundation of Liaoning Province, China (20121068), National Natural Science Foundation of China (No. 21133010, 21261160487, 51221264), National Basic Research Program (973 Program, No.2011CBA00504), and Strategic Priority Research Program of the Chinese Academy of Sciences, Grant No. XDA09030103. We thank Prof. Robert Schlögl from FHI (Berlin) for discussions.

Supporting information for this article is available on the WWW under http://dx.doi.org/10.1002/anie.201410093.

three kinds of CNTs (CNT7000, CNT9000, and HHT) with different diameters was investigated to study the influence of curvature. The TEM images are shown in Figure S1 of the Supporting Information. The average diameters for CNT7000, CNT9000, and HHT were 6–8 nm, 10 nm, and 100 nm, respectively. As shown in Figure S2, CNT7000 gave the highest phenol yield of 5.8%, while the lowest phenol yield of 0.2% was obtained on HHT. It seemed that high phenol yield was due to the small diameter, which is similar to results reported elsewhere.[11c] However, we found from the high-resolution TEM images (Figure S3) that the surface structure of these CNTs was quite different, thus the effect of surface physicochemical properties could not be simply neglected.

HHT is a typical CNT which is treated up to 2700 °C hand has a well graphitized form, the metal content (Fe) is less than 100 ppm. We chose HHT in the subsequent study because the amount of the intrinsic defects on this carbon nanotube was very small, it was favorable for studying the effect of HNO_3 oxidation on the defects. This sample was pre-treated with concentrated HCl at room temperature for 20 h to further reduce the Fe residue before use. The HHT was then oxidized by concentrated HNO_3 at 120, 140, or 160 °C, respectively, the resulting catalysts were denoted HHT120, HHT140, and HHT160, respectively. The temperatures given are the temperatures of the oil bath. As shown in Table S1, the surface area of HHT was slightly increased by the treatment in HNO_3, while the pore volume and average pore size were not obviously changed. The catalytic performance of these CNTs is summarized in Figure 1. They phenol yield is very low, but it

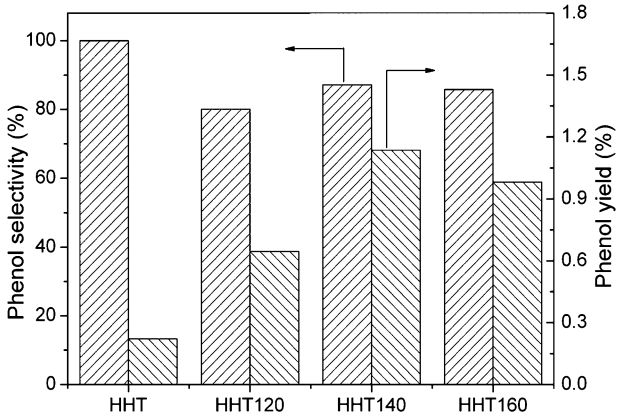

Figure 1. Catalytic performance of HHT and HNO_3-oxidized HHT. Reaction conditions: 60 °C, 6 h, 50 mg catalyst, 0.5 mL benzene, 10 mL acetonitrile, H_2O_2/benzene molar ratio is 2.

increases after the HNO_3 treatment at 120 °C and 140 °C. The yield decreased when treated at the higher temperature of 160 °C.

HNO_3 oxidation is a common method to functionalize carbon materials with oxygenated groups and increase the density of surface defects.[1b,11b,d,e] As expected, XPS spectra indicated that the surface of HHT was efficiently functionalized with oxygenated groups by HNO_3 treatment (Figure S4 and Figure S5). The O1s spectra were deconvoluted into 3 peaks, which appeared around 531.4 eV, 532.5 eV, and 533.7 eV, they were assigned to C=O, O=C–O, and C–OH groups respectively.[7b] Of these three species, only the content of C=O groups increased with treatment temperatures up to 140 °C (Table 2 and Figure S6), indicating the carbonyl group might have positive effect on the phenol yield.

Table 2: Summary of XPS O1 s data.[a]

Catalyst	Total [at%]	C=O [at%]	O=C–O [at%]	C–OH [at%]
HHT	1.38	0.03	0.75	0.59
HHT120	2.25	0.25	0.88	1.12
HHT140	2.89	0.74	1.08	1.07
HHT160	2.49	0.29	1.12	1.08

[a] Species abundance is given in atomic percentage.

The intensity ratio I_{D1}/I_G in the Raman spectra, usually used to indicate the density of defects,[11b,12] increased slightly after the HHT was oxidized at 120 °C, but increased significantly at higher temperatures (Figure S7). The phenol yield exhibited a nearly linearly dependence on the I_{D1}/I_G ratio (Figure 2), indicating that the defects had a critical influence

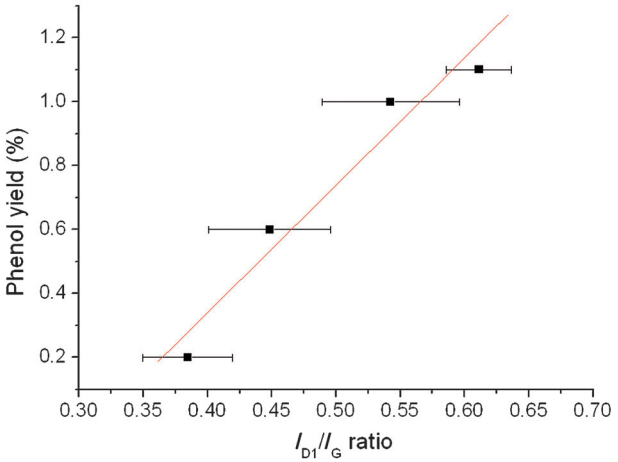

Figure 2. Phenol yield as a function of I_{D1}/I_G.

on the activity of the carbon catalysts. The TEM images of these HHT catalysts are shown in Figure 3. It seems that the surface of HHT140 was rougher than other catalysts, which agreed well with the results from Raman spectra. The boiling point of HNO_3 is about 130 °C, thus the HNO_3 was already boiling when heated at 140 °C and 160 °C in the oil bath. The gas HNO_3 could not be quickly condensed at 160 °C in the oil bath, therefore the treatment at 140 °C in oil bath was more efficient than others to create defects.

Recently, we showed that 9,10-anthraquinone, 1,4-benzenediol, phthalide, benzoic acid, and benzyl ether could be efficiently used as model catalysts to study the roles of carbonyl, phenol, lactone, carboxylic acid, and ether groups in the liquid-phase reactions.[8] In the current study, these small molecules are applied to further investigate the roles of these surface groups (Table 3). However, all these model molecules

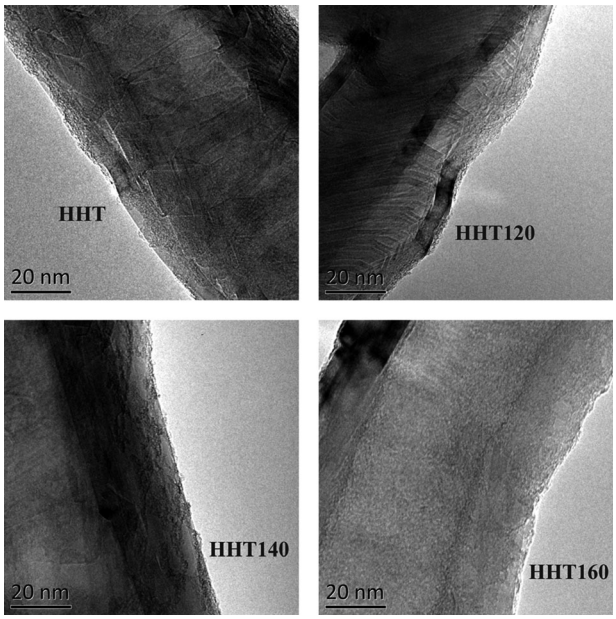

Figure 3. TEM images of HHT, HHT120, HHT140, and HHT160.

Table 3: Performance of model catalysts for benzene oxidation.[a]

Catalysts	Mimicked group/ structure	Phenol yield [%]	Phenol selectivity [%]
Phenanthraquinone	carbonyl	0.3	100
9,10-anthraquinone	carbonyl	0.1	100
1,4-benzenediol	phenol	0.1	100
Phthalide	lactone	0.1	100
Benzoic acid	carboxylic acid	0.1	100
Benzyl ether	ether	0.1	100
Phenanthrene	armchair	0.4	100
Anthracene	zigzag	0.1	100
Blank[b]	-	-	-

[a] Reaction conditions: 60 °C, 6 h, 50 mg catalyst, 0.5 mL benzene, 10 mL acetonitrile, H_2O_2/benzene molar ratio is 2. [b] Conducted in the absence of catalyst: no phenol was detected.

showed negligible phenol yield, indicating oxygenated functional groups did not play a critical role in this reaction, which did not support our above mentioned assumption that the carbonyl group might have a positive effect. The UV detector is very sensitive to the phenol concentration, the subtle difference in phenol yield could be clearly distinguished (no phenol was detected in the blank experiment in the absence of any catalyst). Although many reactions were reported to be catalyzed by defects,[1b,11b,13] it is a challenge to identify which type of defects were the actual active sites as there were many types of defects. Recently, it was successfully demonstrated by first-principles calculations that a particular structure of a nitrogen pair doped Stone–Wales defect provided a good active site in the oxygen reduction reaction (ORR),[13] however it was very difficult to identify the specific structure of the active defects by experiment. To study the roles of specific defect, we used two model catalysts phenanthrene and anthracene to mimic two types of defects namely armchair and zigzag edge, respectively. It was found (Table 3) that phenanthrene gave a much higher phenol yield than anthracene, indicating the armchair configuration might have some positive influence on the reaction.

From the quasi in situ ATR-IR spectra (Figure S8), clear peaks appeared (1046–1328 cm^{-1}) during the oxidation treatment on the phenanthrene, and these peaks could be assigned to C-O-C stretches,[14] which directly indicating that active oxygen species were formed during the reaction. The B band $\pi\rightarrow\pi^*$ transition of phenanthrene in the quasi in situ UV spectra also support this conclusion. This peak, located at 376 nm, gradually weakened during the oxidation treatment, while a shoulder around 355 nm appeared (Figure S9). This shoulder was similar to that resulting from the oxygenated groups in the polycyclic aromatics,[15] indicating there might be a strong interaction between the oxidant and phenanthrene. It seems that armchair configuration was more favorable to interact with the oxidant because the adsorption energy of oxidant on the armchair configuration, obtained from the DFT calculations, was lower (Figure S10). The H_2O_2 decomposition experiment indicated that the interaction between armchair edge and oxidant was stronger than that between zigzag edge and oxidant (Figure S11).

SIMS was an effective tool to characterize the surface structure. It is capable of detecting the first atomic layers of carbon materials, as well as profiling all ejected fragments from the surface during the bombardment of high energy ions. The SIMS spectra in Figure S12 show intense peaks arising from negatively charged C_2H^-, $C_2H_2^-$, and C_2^- fragment ions. The C_2H^- and C_2^- fragments are regarded as good measures of the aromatic C–H groups and aromatic/graphitic carbon, respectively.[16] The ratio of the C_2H^-/C_2^- peak is reported to be a direct measure of the surface concentration of aromatic C–H groups and thus it gives the inverse of the size of aromatic system.[16] It was found that the signal of $C_2H_2^-$ as an acetylene-like fragment increased with the surface erosion time,[17] which was helpful to describe the hydrogenated defects in the graphitic matrix. Recently, we successfully described the surface defects based on the $C_2H_2^-/C_2^-$ ratio, and found that the defects were the active sites during the methane decomposition over carbon nanomaterials.[16d] Herein, the phenol yield was also correlated with the $C_2H_2^-/C_2^-$ ratio (Figure 4), the phenol yield increased with the increase in the$C_2H_2^-/C_2^-$ ratio, indicating that the defects might have a positive effect on this oxidation reaction, which was in accordance with the results from Raman spectra.

Based on the above results and related work,[11a,b,c] we think that H_2O_2 molecules chemisorb on the defect sites during the reaction, and then form intermediate active oxygen species. The active oxygen species attack the adjacent benzene molecule which is adsorbed on the carbon surface through the π–π interaction, and phenol is formed. As we known, there are many types of defects. Although we could not identify the specific structure of the active defect sites, it could be assumed that the only defects that were favorable for the formation of active oxygen species were the armchair edges.

Although the maximum phenol yield in our study was only 5.8% (CNT7000), it could be optimized by varying the reaction conditions. For instance, the phenol yield could be

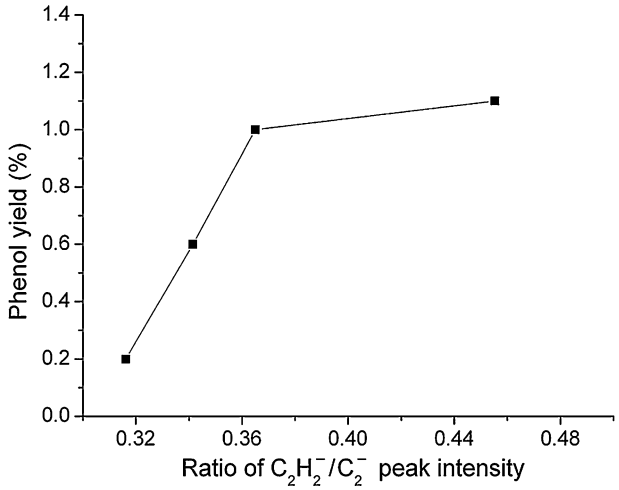

Figure 4. Relationship between the ratio of $C_2H_2^-/C_2^-$ peak intensity and phenol yield.

improved to 10.7% when we added 1 mL benzene and 100 mg catalysts, and could be further increased to 13.7% when we prolonged the reaction time to 36 h (Figure S13). We did not increase the ratio between H_2O_2 and benzene to optimize the phenol yield as the stoichiometry number was only 0.5. Although it was reported that a higher phenol yield of 18% could be obtained,[11a] a much higher amount of H_2O_2 was added (the molar ratio of H_2O_2 to benzene was as high as 12.7.

In summary, an insight into the mechanism of the direct oxidation of benzene to phenol over carbon catalysts was proposed by using model catalysts, Raman spectra, SIMS, quasi in situ ATR-IR, and UV spectra. It was found that defects that could activate oxygen were the active sites. The armchair configuration defect was successfully identified to be one type of active site. Model catalysts, Raman spectra, SIMS and quasi in situ IR and UV spectra were demonstrated to be very direct and effective to investigate the defect sites, which will shed some light on the mechanism of the carbocatalysis.

Experimental Section

The flake graphite (bought from Alfa Aesar) with average particle sizes of 7–10 μm was denoted as FG7–10. CNT7000 and CNT9000 were bought from CNano Technology Limited, they represented FloTube 7000 and FloTube 9000 carbon nanotubes, respectively. HHT was bought from Pyrograf Products, Inc. All the three carbon nanotubes were pretreated in concentrated HCl at room temperature for 20 h to reduce the metal impurities before use. Then, the HHT was heated under reflux in concentrated HNO_3 at 120, 140, and 160 °C in an oil bath for 2 h (the temperatures given are the temperatures of the oil bath), washed to neutral with deionized water, and finally dried at 120 °C overnight. The as-prepared catalysts were named HHT120, HHT140, and HHT160, respectively.

The specific surface area was measured by the Brunauer–Emmett–Teller (BET) method using nitrogen adsorption–desorption isotherms on a Micrometrics ASAP 2020 system. Pore size distributions were estimated from the desorption branches of the isotherms using the Barrett–Joyner–Halenda (BJH) method. The total pore volumes (V_P) were estimated on the basis of the amount adsorbed at a relative pressure of 0.99. Transmission electron microscopy (TEM) images were recorded on a FEI Tecnai T12 with an accelerating voltage of 120 kV. The X-ray photoelectron spectroscopy (XPS) spectra were carried out on an ESCALAB 250 XPS system with a monochromatized $Al_{K\alpha}$ X-ray source. The C1s peak was not deconvoluted because the deconvolution of the C1s peak is generally more difficult and ambiguous, as the contribution from the oxygenated groups compared to that from the asymmetrically shaped graphitized carbon signal is too small to be isolated directly from the spectra.[18] Raman spectroscopy were recorded with a LabRam HR 800 using 633 nm laser. Static secondary ion mass spectroscopy (SIMS) with a TOF-SIMS V instrument was carried out at 500 μm × 500 μm (128 × 128) pixels region with 30 keV electron beam.

The benzene oxidation reaction was carried out in a flask equipped with a reflux condenser under atmospheric pressure in the presence of benzene (0.5 mL), 30% H_2O_2 (1.2 mL), acetonitrile (10 mL), and catalyst (50 mg) at 60 °C for 6 h. The products were analyzed by HPLC (Elite, UV detector, mobile phase: 60/40 (v/v) methanol/water) with SinoChrom ODS-BP column. As phenol (P) and benzoquinone (B) were the only two detected liquid products, the phenol selectivity (S_p) was defined as the mole of phenol produced normalized by the total mole of phenol and benzoquinone liquid products. As most of the related references did not use the phenol formation rate but phenol yield to describe the activity of the catalysts, we also use the phenol yield in this study for comparison.

Keywords: benzene · carbon · model catalysts · phenol · static secondary ion mass spectroscopy

How to cite: *Angew. Chem. Int. Ed.* **2015**, *54*, 4105–4109
Angew. Chem. **2015**, *127*, 4178–4182

[1] a) J. Zhang, X. Liu, R. Blume, A. H. Zhang, R. Schlögl, D. S. Su, *Science* **2008**, *322*, 73–77; b) D. S. Su, S. Perathoner, G. Centi, *Chem. Rev.* **2013**, *113*, 5782–5816; c) M. F. R. Pereira, J. J. M. Órfão, J. L. Figueiredo, *Appl. Catal. A* **1999**, *184*, 153–160; d) C. D. Liang, H. Xie, V. Schwartz, J. Howe, S. Dai, S. H. Overbury, *J. Am. Chem. Soc.* **2009**, *131*, 7735–7741.

[2] a) Y. J. Gao, G. Hu, J. Zhong, Z. J. Shi, Y. S. Zhu, D. S. Su, J. G. Wang, X. H. Bao, D. Ma, *Angew. Chem. Int. Ed.* **2013**, *52*, 2109–2113; *Angew. Chem.* **2013**, *125*, 2163–2167; b) H. Yu, F. Peng, J. Tan, X. W. Hu, H. J. Wang, J. Yang, W. X. Zheng, *Angew. Chem. Int. Ed.* **2011**, *50*, 3978–3982; *Angew. Chem.* **2011**, *123*, 4064–4068.

[3] a) Y. M. Lin, D. S. Su, *ACS Nano* **2014**, *8*, 7823–7833; b) D. R. Dreyer, H. P. Jia, C. W. Bielawski, *Angew. Chem. Int. Ed.* **2010**, *49*, 6813–6816; *Angew. Chem.* **2010**, *122*, 6965–6968; c) Y. B. Kuang, N. M. Islam, Y. Nabae, T. Hayakawa, M. Kakimoto, *Angew. Chem. Int. Ed.* **2010**, *49*, 436–440; *Angew. Chem.* **2010**, *122*, 446–450.

[4] P. R. Chen, L. M. Chew, A. Kostka, K. P. Xie, M. Muhler, W. Xia, *J. Energy Chem.* **2013**, *22*, 312–320.

[5] F. Z. Su, S. C. Mathew, G. Lipner, X. Z. Fu, M. Antoniett, S. Blechert, X. C. Wang, *J. Am. Chem. Soc.* **2010**, *132*, 16299–16301.

[6] D. W. Wang, D. S. Su, *Energy Environ. Sci.* **2014**, *7*, 576–591.

[7] a) D. Chen, A. Holmen, Z. J. Sui, X. G. Zhou, *Chin. J. Catal.* **2014**, *35*, 824–841; b) W. Qi, W. Liu, B. S. Zhang, X. M. Gu, X. L. Guo, D. S. Su, *Angew. Chem. Int. Ed.* **2013**, *52*, 14224–14228; *Angew. Chem.* **2013**, *125*, 14474–14478.

[8] S. C. Wu, G. D. Wen, X. M. Liu, B. W. Zhong, D. S. Su, *ChemCatChem* **2014**, *6*, 1558–1561.

[9] a) S. Niwa, M. Eswaramoorthy, J. Nair, A. Raj, N. Itoh, H. Shoji, T. Namba, F. Mizukami, *Science* **2002**, *295*, 105–107; b) S. Navalon, A. Dhakshinamoorthy, M. Alvaro, H. Garcia, *Chem. Rev.* **2014**, *114*, 6179–6212; c) P. Borah, X. Ma, K. T. Nguyen, Y. L. Zhao, *Angew. Chem. Int. Ed.* **2012**, *51*, 7756–7761; *Angew. Chem.* **2012**, *124*, 7876–7881; d) G. B. Shul'pin, D. V. Muratov,

L. S. Shul'pina, A. R. Kudinov, T. V. Strelkova, P. V. Petrovskiy, *Appl. Organomet. Chem.* **2008**, *22*, 684 – 688.
[10] G. Centi, S. Perathoner, *Catal. Today* **2009**, *143*, 145 – 150.
[11] a) J. H. Yang, G. Sun, Y. J. Gao, H. B. Zhao, P. Tang, J. Tan, A. H. Lu, D. Ma, *Energy Environ. Sci.* **2013**, *6*, 793 – 798; b) S. Q. Song, H. X. Yang, R. C. Rao, H. D. Liu, A. M. Zhang, *Catal. Commun.* **2010**, *11*, 783 – 787; c) Z. H. Kang, E. B. Wang, B. D. Mao, Z. M. Su, L. Gao, L. Niu, H. Y. Shan, L. Xu, *Appl. Catal. A* **2006**, *299*, 212 – 217; d) C. H. Chen, J. Q. Xu, M. M. Jin, G. Y. Li, C. W. Hu, *Chin. J. Chem. Phys.* **2011**, *24*, 358 – 364; e) J. Q. Xu, H. H. Liu, R. G. Yang, G. Y. Li, C. W. Hu, *Chin. J. Catal.* **2012**, *33*, 1622 – 1630.
[12] A. Sadezky, H. Muckenhuber, H. Grothe, R. Niessner, U. Pöschl, *Carbon* **2005**, *43*, 1731 – 1742.
[13] G. L. Chai, Z. F. Hou, D. J. Shu, T. Ikeda, K. Terakura, *J. Am. Chem. Soc.* **2014**, *136*, 13629 – 13640.
[14] R. Wang, X. Y. Sun, B. S. Zhang, X. Y. Sun, D. S. Su, *Chem. Eur. J.* **2014**, *20*, 6324 – 6331.
[15] a) A. M. Jacob, R. K. Thumpakkara, S. Prathapan, B. Jose, *Tetrahedron* **2005**, *61*, 4601 – 4607; b) K. E. Hammel, B. Kalyanaraman, T. K. Kirk, *J. Biol. Chem.* **1986**, *261*, 16948 – 16952; c) M. Diepens, P. Gijsman, *Polym. Degrad. Stab.* **2007**, *92*, 397 – 406.
[16] a) H. Darmstadt, L. Sümmchen, U. Roland, C. Roy, S. Kaliaguine, A. Adnot, *Surf. Interface Anal.* **1997**, *25*, 245 – 253; b) H. Darmstadt, A. Chaala, C. Roy, S. Kaliaguine, *Fuel* **1996**, *75*, 125 – 132; c) P. Albers, K. Deller, B. M. Despeyroux, A. Schäfer, K. Seibold, *J. Catal.* **1992**, *133*, 467 – 478; d) B. W. Zhong, J. Zhang, B. Li, B. S. Zhang, C. L. Dai, X. Y. Sun, R. Wang, D. S. Su, *Phys. Chem. Chem. Phys.* **2014**, *16*, 4488 – 4491.
[17] P. W. Albers, H. Klein, E. S. Lox, K. Seibold, G. Prescher, S. F. Parker, *Phys. Chem. Chem. Phys.* **2000**, *2*, 1051 – 1058.
[18] D. Rosenthal, M. Ruta, R. Schlögl, L. Kiwi-Minsker, *Carbon* **2010**, *48*, 1835 – 1843.

Received: October 14, 2014
Revised: December 2, 2014
Published online: February 3, 2015

